J. Fluid Mech. (2005), *vol.* 534, *pp.* 227–236.
doi:10.1017/S0022112005004763 Printed in the United Kingdom

A new law of thinning in foam dynamics

By L. N. BRUSH[1] AND S. H. DAVIS[2]

[1]Department of Materials Science and Engineering, University of Washington, Seattle, WA 98195, USA

[2]Department of Engineering Sciences and Applied Mathematics, Northwestern University, Evanston, IL 60208, USA

(Received 2 December 2004 and in revised form 7 April 2005)

A new law for the thinning of surfactant-free lamellae (applicable to metallic and ceramic foams with mobile interfaces) in a cross-section of an arid gas–liquid foam is derived using matched asymptotic analysis. Two limiting cases are identified at small capillary number: the well-known semi-arid foam having unit-order liquid fraction and the arid foam in which it is small. The lamellar thinning rates in both cases exhibit t^{-2} power-law behaviour at long times even though the foam liquid area fractions have different orders of magnitude in capillary number. At early times, arid foam thinning is slowed because the curvature of the capillary quasi-static interfacial region must decrease in order to accommodate the flow from the films. Therefore, the thinning of lamellae feeding into a given Plateau border is coupled and the dynamics is distinct from that of the semi-arid foam.

Approximations of rupture times in arid and semi-arid foams are found by calculating the times for lamellae to thin to a pre-specified thickness. For given initial lamellar thicknesses, and for arid and semi-arid foams that have identical initial lamellar liquid areas, the arid foam ruptures more quickly than the semi-arid foam. On the other hand the rupture of lamellae is significantly delayed in arid foam compared to semi-arid foam if the initial lamellar thickness and capillary number are the same.

1. Introduction

A foam is composed of gas bubbles in a liquid, the bubbles being polygonal due to crowding if the mass fraction of liquid is small enough. The bubbles are separated from each other by thin liquid films connected by junctions. The lifetime of a foam is determined by the thinning and the rupture of the films, resulting in the coalescence of adjacent bubbles into, ultimately, a single gas bubble in a liquid bath. This process occurs in parallel with the draining of liquid along the axes of the lamellar junctions, a process driven by gravity and ignored in the present analysis. The thinning and rupture processes stand as the fundamental building blocks of a theory of the behaviour of foams on the large scale.

For pure metallic or water-like liquids, the rupture times can be measured in milliseconds. In aqueous foams the films are laden with surfactants to immobilize the interfaces and hence to slow the rupture of the films by orders of magnitude, as detailed in the work of Breward (1999) and Breward & Howell (2002). In metallic foams surfactants are ineffective and only some control of the viscosity of the liquid metal can slow the process. For example, alumina particles are dispersed in aluminium foam to increase the viscosity and decrease the drainage sufficiently so that solidification can occur (Yang & Nakae 2003), though the addition of impurities to the melt, a

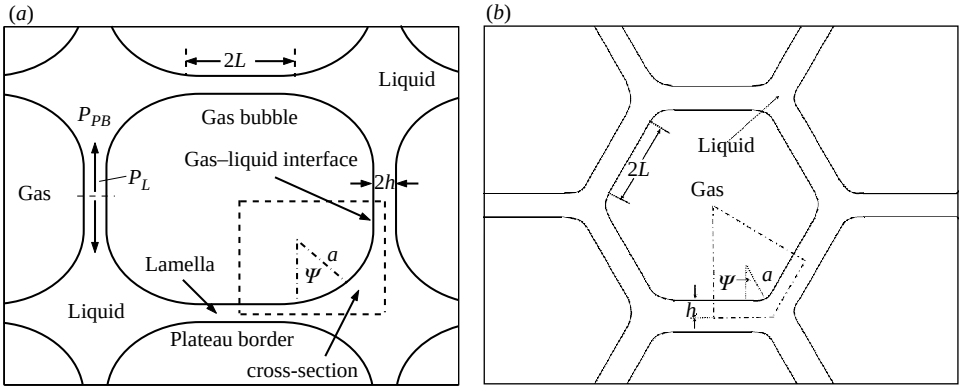

FIGURE 1. Schematic representation of the cross-sections of foams for (a) a square array and (b) an hexagonal array of bubbles showing a set of adjacent gas bubbles and the lamellar (L), transition (T) and Plateau border (PB) regions. The dot-dash lined sections within each diagram are the periodic domains within which asymptotic analyses are carried out for each geometry. The symmetry of the array of bubbles fixes the angle $\Psi : \Psi = \pi/4$ in (a) and $\pi/6$ in (b).

common practice in processing of gas–liquid metallic foams, is not a generally viable technique. Finally, in highly viscous melts such as molten glass, rupture times of thin films can be many orders of magnitude longer as shown by Howell (1999) in a study of the drainage of a bubble.

The foam considered in this work is surfactant free and has an area fraction of liquid of a couple of percent or less. At these small liquid fractions, within the foam between polygonal bubbles, the liquid forms elongated thin-film regions, lamellae (L), separated by rounded regions of (nearly) constant curvature, Plateau border cross-sections (PB). Liquid flows from the higher pressure L regions to the lower pressure PB regions promoting continuous L thinning. Breward & Howell (2002) have analysed foam thinning and have estimated thinning times in foam both with and without surfactant, in the absence of gravitational drainage. In their work, the radius of curvature of the PB is assumed fixed, which describes the semi-arid foam in the low-capillary-number asymptotic limit. For smaller liquid fractions at leading order in the asymptotic analysis, the PB radius of curvature must be allowed to increase in time in order that liquid be conserved within a two-dimensional cross-section. This leads to the arid limit which has different lamellar thinning dynamics.

In the present work asymptotic solutions within a cross-section of foam are determined, in which the dynamics of the geometrical features, such as the radius of curvature of the PB, and the length and the thickness of the lamella that fully characterize the foam geometry, are determined as part of the solution to the problem. This is accomplished by considering conservation of liquid and strict periodicity of the array of bubbles within the two-dimensional cross-section.

In figure 1 are schematic diagrams of the types of arrays of passive gas bubbles and surrounding liquid regions that are considered in this work. Figure 1(a) is a square array of bubbles which in general is not observed but serves as illustration. Figure 1(b) shows an hexagonal array of bubbles which is commonly seen in foams. Our theory applies to either geometry. No drainage is allowed orthogonal to the PB cross-sectional areas in this analysis.

The gas bubbles are assumed to form a periodic array in space. Therefore, it is possible to characterize microscale flow and interface evolution by focusing on a

periodic domain denoted as the region contained within the dashed line in figure 1(*a*) and within the dot-dash line in figure 1(*b*). A domain includes one 'corner' of a gas bubble along with the adjacent PB and L liquid regions. In figure 1 four geometrical parameters are depicted: the PB radius of curvature a, the lamellar thickness $2h$, the lamellar length $2L$ and Ψ, an angle which is set by the symmetry of the bubble array. These geometrical factors completely characterize the geometry of the foam at the microscale in this analysis, and because of periodicity, also at the macroscale.

The area fraction of the liquid and the size of the PB, L and transition (T) regions are functions of the geometrical parameters. These quantities vary significantly depending on the foam processing method, of which there is a variety. It is therefore crucial to examine the dependence of the dynamics of foam on these geometrical parameters since this is linked to the processing technique.

The results of this work reveal fundamental differences in foam dynamics, including L thinning and the dynamics of PB interfaces, depending on the ratios of the foam geometrical parameters.

2. The model

The equations governing change in the components of the liquid velocity ($u(x, z, t)$, $w(x, z, t)$) and the pressure $p(x, z, t)$ are

$$\rho(u_t + uu_x + wu_z) = -p_x + \mu(u_{xx} + u_{zz}), \tag{2.1}$$

$$\rho(w_t + uw_x + ww_z) = -p_z + \mu(w_{xx} + w_{zz}), \tag{2.2}$$

$$u_x + w_z = 0, \tag{2.3}$$

where ρ and μ are the density and viscosity of the liquid. At the gas–liquid interface $z = h(t, x)$ the kinematic condition is written

$$w = h_t + uh_x. \tag{2.4}$$

The normal stress at the interface obeys

$$-p + P_G + \frac{2\mu}{\left(1 + h_x^2\right)}\left[\left(u_x h_x^2 + w_z\right) - h_x(u_z + w_x)\right] = \sigma \frac{h_{xx}}{\left(1 + h_x^2\right)^{3/2}}, \tag{2.5}$$

where P_G is the hydrostatic pressure in the passive gas phase and σ is the gas–liquid surface tension. The shear stress at the gas–liquid interface vanishes:

$$-2\mu(u_x - w_z)h_x + \mu(u_z + w_x)\left(1 - h_x^2\right) = 0. \tag{2.6}$$

The free film is assumed to be symmetric about the coordinate contour $z = 0$, and along the centreline, $u_z = 0$ and $w = 0$. (For a general review of models of thin films including a wide variety of physical effects, see Oron, Davis & Bankoff (1997).)

Within PBs, flow and interface shape are controlled by capillary effects whereas in L regions by viscous effects. Separate asymptotic solutions for the flow of liquid and the dynamics of the gas–liquid interface are calculated for each region. However, the leading-order solutions within the adjacent PB and L regions can only be matched by introducing an intermediate transition region (T), as done initially by Bretherton (1961). The solutions within each of the L, T and PB regions are considered in the subsections below.

2.1. *The Plateau borders*

Governing equations appropriate for the capillary static region are derived by transforming (2.1) to (2.6) according to

$$(\tilde{x},\tilde{z})=\left(\frac{x}{L_o},\frac{z}{L_o}\right),\quad (\tilde{u},\tilde{w})=\left(\frac{u}{U_o},\frac{w}{U_o}\right),\quad \tilde{t}=\left(\frac{U_o}{L_o}\right)t,\quad \tilde{P}=\left(\frac{L_o}{\sigma}\right)p, \tag{2.7}$$

where L_o is the initial lamella half-length, and U_o is a velocity which will be determined as part of the solution to the problem. To leading order in capillary number $C=\mu U_o/\sigma$ the governing equations are reduced to a single equation for the shape:

$$-\Delta\tilde{P}=\frac{\tilde{h}_{\tilde{x}\tilde{x}}}{\left(1+\tilde{h}_{\tilde{x}}^2\right)^{3/2}}. \tag{2.8}$$

$\Delta\tilde{P}$ is a constant jump in pressure across a gas–liquid interface of constant curvature. A solution is found by integrating the leading-order ($C=0$) set of equations. For any array of gas bubbles the solution is a circular arc. The span or total arc of the PB region is fixed by the angle Ψ which is dictated by the symmetry of the array; an array with an n-fold rotational axis must satisfy $n=\pi/\Psi$. For bubble centres configured as a two-dimensional square lattice the interface shape is

$$\tilde{h}(\tilde{x},\tilde{t})=\tilde{h}_o+\tilde{a}\left(1-\frac{\sqrt{2}}{2}\right)-\frac{1}{\sqrt{2}\Delta\tilde{P}}+\frac{1}{\Delta\tilde{P}}\left[1-\left(\frac{1}{\sqrt{2}}-\Delta\tilde{P}\left[\tilde{x}-\tilde{L}-\frac{1}{\sqrt{2}}\tilde{a}\right]\right)^2\right]^{1/2} \tag{2.9}$$

where $\tilde{h}_o$ is an undetermined constant. The parameters $\tilde{L}$ and $\tilde{a}$ are the dimensionless lamellar length and radius of curvature, respectively. The solution (2.9) obeys the symmetry conditions

$$\tilde{h}_{\tilde{x}}=1\quad \text{at } \tilde{x}=S\{\tilde{t}\}:=\tilde{L}+\frac{\tilde{a}}{\sqrt{2}} \tag{2.10}$$

and

$$\tilde{h}=\tilde{h}_o+\tilde{a}\left(1-\frac{1}{\sqrt{2}}\right)\quad \text{at } \tilde{x}=S\{\tilde{t}\}:=\tilde{L}+\frac{\tilde{a}}{\sqrt{2}}. \tag{2.11}$$

The values of ΔP and $\tilde{h}_o$ and $\tilde{a}$ are related by means of matching conditions with the T solution, and through conservation of liquid. First, the solutions in the thin-film L and T regions must be determined.

2.2. *Thin-film regions: lubrication approximation*

In order to determine the flow and interface evolution in the thin-film regions between adjacent gas bubbles away from the PB where viscous effects are important and the lubrication approximation is valid, variable rescaling is required. The analysis of this section is similar in spirit to that of Breward & Howell (2002).

The thin-film region may be subdivided into lamellar (L) and transition (T) regions. The T region lies between the PB and L regions. Let $\epsilon=h_o/L_o\ll 1$ be the ratio of the length by which (dimensional) z is scaled to the length by which (dimensional) x is scaled. The coordinate shift $L^*(T)$ and the coordinate stretching parameter δ are defined below. The variable transformations

$$\left.\begin{aligned} &X=\frac{x-L^*(T)}{\delta L_o},\quad Z=\frac{z}{h_o},\quad T=\frac{tU_o}{L_o},\quad U=\frac{u}{U_o},\\ &W=\frac{wL_o}{h_oU_o},\quad P=\frac{\epsilon^2L_o}{\mu U_o}p,\quad H=\frac{h}{h_o} \end{aligned}\right\} \tag{2.12}$$

convert (2.1)–(2.6) to a form appropriate for a free film. The result is a coupled set of equations for the axial component of the fluid velocity $U(X, T)$ and the interface shape $H(X, T)$:

$$H_T + \frac{1}{\delta}((U - L_T^*)H)_X = 0, \tag{2.13}$$

$$-\left(\frac{C^{-1}\epsilon}{\delta^3}\right) H H_{XXX} = \frac{4}{\delta^2}(HU_X)_X. \tag{2.14}$$

Inertial effects are assumed negligible. All other quantities derive from $U(T, X)$ and $H(T, X)$. The choice $\delta = 1$ and $L^*(T) = 0$ gives a set of equations appropriate for the L region. In the T region viscous and capillary forces balance only if the X coordinate is stretched by $\delta = \epsilon/C$, so that $\epsilon \ll \delta \ll 1$. It follows that $U_o = (\sigma/\mu)(h_o/a_o)^{1/2}$, where a_o is the initial radius of the PB region. With this choice of δ and the choice $L^*(T) = L(T)$ a set of equations appropriate for the T region is given.

In the L region the appropriate solution is a flat interface $H(T)$ that obeys

$$\frac{\mathrm{d}H_L}{\mathrm{d}T} = -\frac{\overline{Q}(T)}{L(T)}, \tag{2.15}$$

where $\overline{Q}(T) = U(L, T)H(T)$ is the liquid flow rate at the L/T border. $U(T, X) = \overline{Q}X/(LH_L)$ is the fluid velocity throughout the L region. The flow rate $\overline{Q}$, which is not known *a priori*, will be determined by matching at the T/PB border.

From (2.13) and (2.14) it is seen that the leading-order solution in the T region is quasi-static. These equations may be integrated and matched at both the L/T border and at the T/PB border. The results show that the transition solution has the same thickness as the lamella and a vanishing slope at the L border. Matching also reveals that to leading order the PB circular arc joins the adjacent lamellar regions by fitting exactly into the corner formed by the centrelines of two adjacent intersecting lamellae. Thus $\Delta\tilde{P} = -1/\tilde{a}$ and $\tilde{h}_o = 0$ in (2.9). Finally the matching conditions also link the constant flow rate $\overline{Q} = UH$ at any time through the T region to the radius of curvature of the PB region:

$$\frac{1}{2}\left(\frac{8}{3}\right)^2 \frac{\overline{Q}^2}{H_L^3} = \tilde{h}_{\tilde{x}\tilde{x}}(\tilde{L})\left[\frac{\delta^2}{\epsilon}\right]. \tag{2.16}$$

Here, $\tilde{h}_{\tilde{x}\tilde{x}}(\tilde{L})$ is the curvature, $1/\tilde{a}$, of the PB portion of the interface. This result has been written for $L_T = 0$ which is valid here as will be shown below. Since the quasi-static condition applies, the matching conditions hold at any instant in time.

2.3. *Conservation of fluid and array periodicity*

Designating the leading-order solutions for the L and the PB regions as $h_L(t)$ and $h_{PB}(t, x)$) respectively, the liquid area, written in dimensional form:

$$A = \int_0^{L(t)} h_L(t)\,\mathrm{d}x + \int_{L(t)}^{S(t)} h_{PB}(t)\,\mathrm{d}x + \int_{S(t)}^{d} h_{PB}\{S(t)\}\left(\frac{d-x}{d-S(t)}\right)\mathrm{d}x, \tag{2.17}$$

is constant in time. Here $S\{t\} = L(t) + a\sin\Psi$, the constant length $d = (h_L + a)\tan\Psi + L + \delta L_o$, and a is the radius of curvature of the circular PB region. The contribution to the area of fluid within the T region is higher order compared to the contribution from other regions. The geometry used to derive the conservation law is represented in figure 1(a, b). In the last integrand the value $h_{PB}\{S(t)\}$ refers to the PB solution evaluated at the location $S(t)$. Differentiation and evaluation of (2.17) gives at leading

order:

$$-\frac{1}{2}(\tan\Psi-\Psi)\frac{\mathrm{d}(\overline{a}^2)}{\mathrm{d}\overline{T}}=\frac{\mathrm{d}(H_L\overline{L})}{\mathrm{d}\overline{T}}\left[\frac{L_o h_o}{a_o^2}\right]. \tag{2.18}$$

In addition the requirement that the time rate of change of d vanishes at leading order gives

$$\frac{\mathrm{d}\overline{L}}{\mathrm{d}\overline{T}}=-\left[\frac{a_o}{L_o}\right]\frac{\mathrm{d}\overline{a}}{\mathrm{d}\overline{T}}\sin\Psi. \tag{2.19}$$

The barred quantities are the dimensional variables scaled by corresponding initial values. Initial values of variables are denoted by the subscript 'o'. All dimensionless variables are taken to be $O(1)$.

Given an initial lamellar length, an initial radius of curvature, an initial lamellar thickness, and auxiliary conditions, and noting that $\delta^2 L_o/a_o\epsilon=1$, equations (2.15), (2.16), (2.18) and (2.19) may be integrated to give H_L as a function of time T.

3. Semi-arid and arid foams

The coefficients a_o/L_o and $L_o h_o/a_o^2$, appearing in (2.18) and (2.19), remain to be chosen. Choosing either ratio to be unity represents a distinquished limit.

Semi-arid foam is defined by the choice $a_o/L_o\sim O(1)$. Therefore, $L_o h_o/a_o^2\sim O(\epsilon)$, $\delta=\sqrt{a_o h_o}/L_o\sim O(\epsilon^{1/2})$, the area fraction of liquid is $O(1)$ and the area of fluid in the PB is much greater than in the L region. Given these ratios, then the right-hand side of (2.18) is higher order and the radius of the circular arc is constant in time. It follows from (2.19) that the length of the L region remains constant.

Arid foam is defined by the choice $a_o/\sqrt{L_o h_o}\sim O(1)$. Therefore, $a_o/L_o\sim O(\epsilon^{1/2})$, $\delta\sim O(\epsilon^{3/4})$, $\epsilon/\delta\sim O(\epsilon^{1/4})$, the area fraction of liquid is $O(\epsilon)$ and a balance is struck between fluid areas contained in the PB corner and in the L regions of the foam. Therefore, according to (2.19), $\mathrm{d}L/\mathrm{d}t$ vanishes, so that the length of L is constant. However, from (2.18) there will be a change in the radius of curvature of the PB.

Using these estimates, the governing set of equations can be reduced to a single dynamical equation for the lamellar thickness for both arid and semi-arid foam. Dimensionless L is set to unity, consistent with the results of the previous section. Substituting $\hat{h}=\overline{H}_L/(\omega+1)$ and $\hat{t}=T/t^*$ where $\omega=(1/2)(\tan\Psi-\Psi)$ and $t^*=8\omega^{-1/4}(1+\omega)^{-1/4}/(3\sqrt{2})$ leads to the canonical law of thinning in arid foam

$$\frac{\mathrm{d}\hat{h}}{\mathrm{d}\hat{t}}=-\hat{h}^{3/2}[1-\hat{h}]^{-1/4}, \tag{3.1}$$

with initial condition $\hat{h}(0)=[1/(1+\omega)]$. The solution is

$$\frac{2[1-\hat{h}]^{1/4}+\hat{h}\ F\left(\frac{1}{2},\frac{3}{4};\frac{3}{2};\hat{h}\right)}{\sqrt{\hat{h}}}-\frac{2[1-\hat{h}(0)]^{1/4}+\hat{h}(0)\ F\left(\frac{1}{2},\frac{3}{4};\frac{3}{2};\hat{h}(0)\right)}{\sqrt{\hat{h}(0)}}=\hat{t} \tag{3.2}$$

where F denotes the (Gauss) hypergeometric function. Written in the arid-foam canonical variables, the semi-arid-foam lamellar thickness obeys

$$p^{-1}\frac{\mathrm{d}\hat{h}}{\mathrm{d}\hat{t}}=-\hat{h}^{3/2} \tag{3.3}$$

where $p=[(1+\omega)/\omega]^{1/4}$ and with the same initial thickness. The semi-arid foam result, (3.3) and the solution $\hat{h}=\hat{h}(0)(1+\hat{t}/2(\omega^{1/4}(1+\omega)^{1/4})^{-2}$ are formally identical to the result of Breward & Howell (2002) since the PB radius of curvature is fixed.

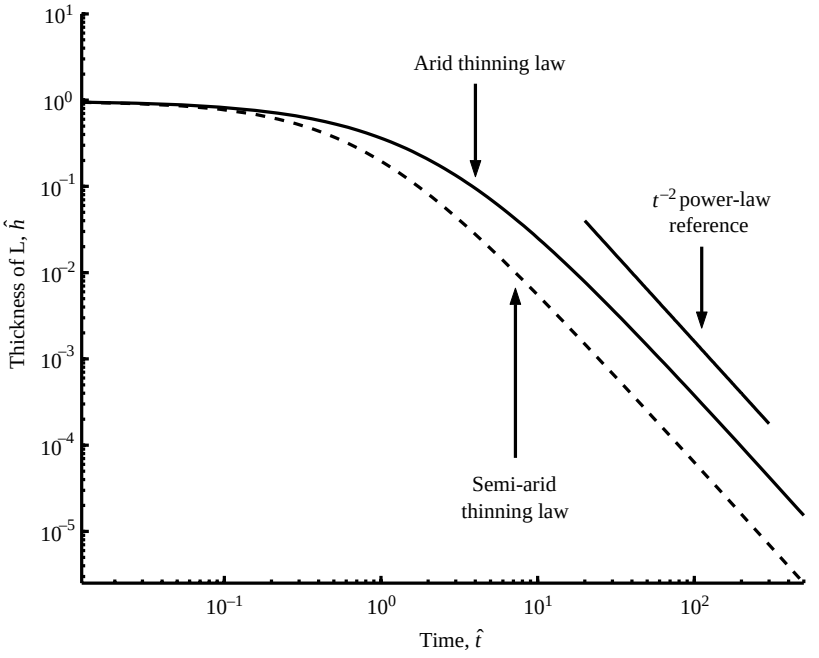

FIGURE 2. Log-log plot of the lamellar thickness of arid (full line) and semi-arid (dashed line) foams as given by the solution to (3.1) and (3.3). The angle Ψ used in the calculations is $\pi/6$ representing lamella joining PBs at orientations $\pi/3$. t^{-2} power-law thinning is indicated by the reference plot.

4. Lamellae thinning and rupture

Figure 2 is a log-log plot of the numerical solutions of (3.1) and (3.3). After an initial transient, the thinning rates are $\hat{h}(\hat{t}) = C_\nu \hat{t}^{-2}$, with constants C_ν referring either to the semi-arid ($\nu = \mathrm{SA}$) or arid ($\nu = \mathrm{A}$) limits. Although at long times the lamella exhibit similar temporal power-law behaviour, the semi-arid and arid foams represent vastly different situations (e.g. different area fractions of liquid phase). In arid foam the thinning behaviour requires an increase in the radius of curvature of the PB that must occur in order that the fluid leaving the L region can be accommodated by the PB region at leading order. Once the PB radius is sufficiently large (or lamella sufficiently thin), $1 - \hat{h} \to 1$, the remaining liquid leaving the L region only affects the PB region at higher order. Figure 3 is a plot of the change in the radius $\hat{a}$ of curvature of the PB and the L thickness $\hat{h}$ in arid foam as a function of time during thinning. In terms of the canonical variables listed above, the radius of curvature of the PB is

$$\hat{a} = (1 - \hat{h})^{1/2} \tag{4.1}$$

where $\hat{a} = \overline{a}\omega^{1/2}/(1+\omega)^{1/2}$. At leading order all fluid flow is driven by the pressure drop which occurs entirely 'locally' across the asymptotically short, $O(\delta)$, transition region. The pressure within the transition region is

$$\hat{P} = \frac{1}{\hat{a}}\left(-1 + \frac{1}{2}\left(\frac{1}{h^*}\right)^{3/2} + \frac{1}{2}\left(\frac{1}{h^*}\right)^{3}\right) \tag{4.2}$$

where dimensionless $\hat{P} = (P - P_G)\delta(1+\omega)^{1/2}/\epsilon^2\omega^{1/2}$, and $h^* = \hat{h}_{TR}/\hat{h}_L$ is the ratio of the T to L thickness, which is unity at the L/T border and vanishes at the T/PB border.

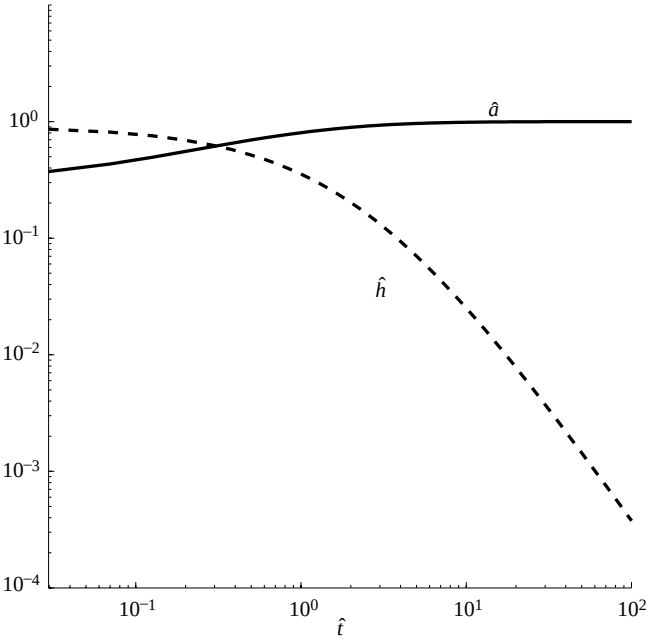

FIGURE 3. Log-log plot of the lamellar thickness (dashed line) and the radius of curvature of the PB (full line) for arid foam as given by the solution of (3.1) and of (4.1). The angle Ψ used in the calculations is $\pi/6$ representing lamella joining PBs at orientations $\pi/3$.

Consequently, the pressure drop across the transition region, i.e. the difference in pressure between the T/PB border and the L/T border, is $\Delta\hat{P} = -1/\hat{a}$. This pressure drop varies with time in arid foam whereas in semi-arid foam the pressure drop across the transition region is constant.

According to (3.1) and (3.3), the lamellar thickness does not vanish in finite time for either the arid or the semi-arid foam. To properly calculate the rupture thickness one needs to solve the linear stability problem for the film with van der Waals attractions, interfacial curvature and flow in the thin film. Instead we obtain a crude estimate based on lamellar thinning only, by choosing a particular value $\hat{h}_r$ of L thickness as a representation of the thickness at rupture.

Numerical solutions to (3.1) and (3.3) provide the dimensionless 'rupture' times for given lamellar thickness. For example, using $\Psi = \pi/6$, corresponding to an hexagonal array, thinning times for thicknesses $\hat{h}_r = 0.1$ and 0.01 in semi-arid (arid) foam are $\hat{t}_r = 1.7589(3.9169)$ and 7.3212 (17.6349), respectively. Interpretation of these results depends on the choice of material system and foam configuration. Two cases are considered. In Case I, the initial L thickness and the initial L length are assumed identical, $\epsilon_{SA} = \epsilon_A$, i.e. the liquid area fractions of the semi-arid and arid foam L regions are initially the same. The difference in fluid area is accounted for entirely by the size of the PB regions. The Case II comparison is between semi-arid and arid foam of equal initial L thicknesses and of equal initial radii of curvature of the PB. This comparison evaluates thinning in arid and semi-arid foam having identical capillary numbers. Table 1 lists the estimated rupture times for Cases I and II in semi-arid and arid foam, for water, aluminium and molten glass. Relevant physical properties are given in the caption. In all cases $h_o = 10^{-7}$ m. For the semi-arid foam, $L_o = 10^{-3}$ m and $a_o = 10^{-3}$ m; in Case I, $L_o = 10^{-3}$ m is the same in both semi-arid and

Foam type	H_2O ($\sim 25^\circ$C)	Al ($> 660^\circ$C)	glass ($\gtrsim 1200^\circ$C)
Semi-arid ($C = 0.01$)	$1.16(\times 10^{-2})$	$3.87(\times 10^{-3})$	$2.03(\times 10^{4})$
Arid (Case I) ($C = 0.1$)	$2.589(\times 10^{-3})$	$8.63(\times 10^{-4})$	$4.53(\times 10^{3})$
Arid (Case II) ($C = 0.01$)	258.9	86.3	$45.3(\times 10^{7})$

TABLE 1. The time (in seconds) it takes for the lamellar thickness to reach 1/10 of its initial value for pure Al, H_2O and molten glass gas–liquid systems. Times are calculated in semi-arid foam for one value of C and in arid foam for two different values of C. The initial lamellar thickness is $h_o = 10^{-7}$ m in all cases. Comparing arid (Case I) with semi-arid foam corresponds to foams having identical initial lamellar dimensions (ϵ fixed) and comparing arid (Case II) with semi-arid foam corresponds to semi-arid and arid-foam both having identical capillary numbers C for a given material. Values of σ and μ are: $\sigma_{H_2O} = 7.0(\times 10^{-2})\,\mathrm{kg\,s^{-2}}$, $\mu_{H_2O} = 10^{-3}\,\mathrm{kg\,m^{-1}\,s^{-1}}$ from Breward & Howell (2002), $\sigma_{Al} = 8.4(\times 10^{-1})\,\mathrm{kg\,s^{-2}}$, $\mu_{Al} = 4.0(\times 10^{-3})\,\mathrm{kg\,m^{-1}\,s^{-1}}$ from Hur, Park & Hiroshi (2003), and $\sigma_{mg} = (\times 10^{-1})\,\mathrm{kg\,s^{-2}}$, $\mu_{mg} = 2.5(\times 10^{3})\,\mathrm{kg\,m^{-1}\,s^{-1}}$ from Howell (1999). Capillary numbers are constant for each foam type and are given in parentheses.

arid foam and in Case II, $a_o = 10^{-3}$ m is the same in both foams. The comparisons are made for $h_r = 10^{-8}$ m ($= 0.1h_o$). In Case I the arid foam ruptures more rapidly than the semi-arid foam, while in Case II it is slower. In table I the capillary numbers are provided for these limiting cases. It can also be shown that the magnitude of the Reynolds numbers indicates that for H_2O and Al in these limiting cases inertia might become important during thinning. For the molten glass the Reynolds number is extremely small and inertia is entirely negligible.

5. Summary

A general model for thinning of surfactant-free foam lamellae has been derived and two distinguished limits for capillary number $C \to 0$ have been identified. Semi-arid foam has $O(1)$ area fraction of liquid and arid foam has $O(C^4)$ area fraction of liquid. In semi-arid foams, defined by the ratio $a_o/L_o = O(1)$, then for small C

$$\frac{h_o L_o}{a_o^2} \sim C^2, \qquad \frac{h_o}{a_o} \sim C^2, \qquad \delta \sim C, \qquad \epsilon \sim C^2.$$

In arid foam, defined by the ratio $h_o L_o/a_o^2 = O(1)$, then for small C

$$\frac{a_o}{L_o} \sim C^2, \qquad \frac{h_o}{a_o} \sim C^2, \qquad \delta \sim C^3, \qquad \epsilon \sim C^4.$$

In both types of foam, the thinness of the transition region ϵ/δ is $O(C)$ and the velocity scale $U_o := \sigma C/\mu = \sigma\epsilon/\mu\delta$. The velocity scale, being proportional to σ/μ, is representative of capillary–viscous thinning.

In figure 4 is a summary of lengths and areas of the L, T and PB regions in terms of the capillary number C. Above the horizontal centreline are the scalings appropriate for the semi-arid foam, which is characterized by the PB radius of curvature and the L length of the same order in C. Below the centreline the scalings for the arid foam are presented. The arid foam is characterized by the initial area of liquid in the L region of the same order in C as the initial area in the corner of a bubble. The thinning rates of L in arid foams differ from those of semi-arid foams due to the increase in the radius of curvature of the quasi-static PB required to accommodate the liquid arriving from the lamellar regions at leading order. Thinning of adjacent

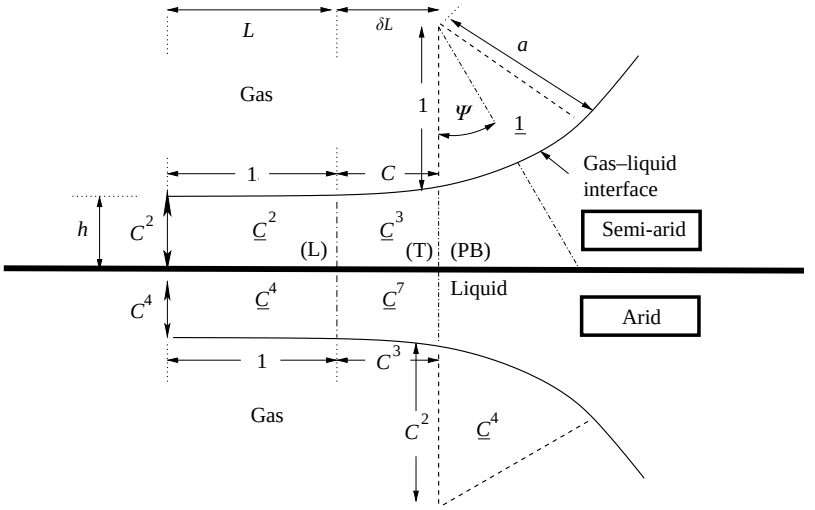

FIGURE 4. Schematic representation of the corners of adjacent gas bubbles and the L, T and PB regions. Dimensional lengths for L, T and the radius of curvature of the PB ($L, \delta L$ and a) are indicated. The lengths and areas of regions are given in terms of capillary number C. Scalings for the semi-arid foam are above the horizontal centreline and for the arid foam are below the centreline. Underlined capillary numbers refer to scalings for areas of liquid and gas regions.

lamellae in arid foams is coupled and depends on the overall geometry of the bubble array and the geometry of the interface in the PB cross-section. Two limiting cases are studied. Rupture of lamellae and bubble coalescence is estimated to be slower in semi-arid foam if both foams have same initial lamellar area, whereas if the PB regions contain the same amount of fluid the arid foam will thin significantly more slowly.

REFERENCES

BRETHERTON, F. P. 1961 The motion of long bubbles in tubes. *J. Fluid Mech.* **10**, 166–188.

BREWARD, C. J. W. 1999 The mathematics of foam. DPhil. thesis, Oxford University.

BREWARD, C. J. W. & HOWELL, P. D. 2002 The drainage of a foam lamella. *J. Fluid Mech.* **458**, 379–406.

HOWELL, P. D. 1999 The draining of a two dimensional bubble. *J. Engng Maths* **35**, 251–272.

HUR, B.-Y., PARK, S.-H. & HIROSHI, A. 2003 Viscosity and surface tension of Al and effects of additional element. *Eco-Materials Processing and Design Materials Science Forum* **439**, 51–56.

ORON, A., DAVIS, S. H. & BANKOFF, S. G. 1997 Long-scale evolution of thin liquid films. *Rev. Mod. Phys.* **69**, 931–980.

YANG, C. C. & NAKAE, H. 2003 The effects of viscosity and cooling conditions on the foamability of aluminum alloy. *J. Mat. Proc. Tech.* **141**, 202–206.